Published in final edited form as:
J Comput Phys. 2010 July ; 229(13): 4996–5010. doi:10.1016/j.jcp.2010.03.021.

An Evaluation of Solution Algorithms and Numerical Approximation Methods for Modeling an Ion Exchange Process

Sunyoung Bu[a,*], **Jingfang Huang**[a], **Treavor H. Boyer**[b], and **Cass T. Miller**[c]

Sunyoung Bu: agatha@email.unc.edu; Jingfang Huang: huang@email.unc.edu; Treavor H. Boyer: thboyer@ufl.edu; Cass T. Miller: caseymiller@unc.edu

[a]Department of Mathematics, University of North Carolina, Chapel Hill, NC 27599-3250

[b]Department of Environmental Engineering Sciences, University of Florida, Gainesville, FL 32611

[c]Department of Environmental Sciences and Engineering, University of North Carolina, Chapel Hill, NC 27599-7431

Abstract

The focus of this work is on the modeling of an ion exchange process that occurs in drinking water treatment applications. The model formulation consists of a two-scale model in which a set of microscale diffusion equations representing ion exchange resin particles that vary in size and age are coupled through a boundary condition with a macroscopic ordinary differential equation (ODE), which represents the concentration of a species in a well-mixed reactor. We introduce a new age-averaged model (AAM) that averages all ion exchange particle ages for a given size particle to avoid the expensive Monte-Carlo simulation associated with previous modeling applications. We discuss two different numerical schemes to approximate both the original Monte Carlo algorithm and the new AAM for this two-scale problem. The first scheme is based on the finite element formulation in space coupled with an existing backward-difference-formula-based ODE solver in time. The second scheme uses an integral equation based Krylov deferred correction (KDC) method and a fast elliptic solver (FES) for the resulting elliptic equations. Numerical results are presented to validate the new AAM algorithm, which is also shown to be more computationally efficient than the original Monte Carlo algorithm. We also demonstrate that the higher order KDC scheme is more efficient than the traditional finite element solution approach and this advantage becomes increasingly important as the desired accuracy of the solution increases. We also discuss issues of smoothness, which affect the efficiency of the KDC-FES approach, and outline additional algorithmic changes that would further improve the efficiency of these developing methods for a wide range of applications.

Keywords

Diffusion Process; Finite Element Methods; Krylov Deferred Correction Methods; Multiscale Modeling; Semi-Implicit Preconditioner

[*]Corresponding author.

Publisher's Disclaimer: This is a PDF file of an unedited manuscript that has been accepted for publication. As a service to our customers we are providing this early version of the manuscript. The manuscript will undergo copyediting, typesetting, and review of the resulting proof before it is published in its final citable form. Please note that during the production process errors may be discovered which could affect the content, and all legal disclaimers that apply to the journal pertain.

1. Introduction

An important research topic and application in drinking water treatment is the effective removal of dissolved organic carbon (DOC). It is well known that DOC contributes taste, odor, and color to raw drinking water; reacts with chlorine to form disinfection byproducts; and fouls membrane filtration systems. There are a variety of processes that can be used to remove DOC. An advanced DOC removal process is ion exchange resin treatment in a completely mixed flow reactor (CMFR), which has been shown to be more effective than traditional coagulation processes [2,22,24]. The ion exchange process operates as shown schematically in Fig. (1): raw water and ion exchange resin are mixed in a CMFR; the treated water exits the reactor; a majority of the ion exchange resin is continuously recycled within the reactor; and a small fraction of ion exchange resin is removed from the reactor, regenerated to restore exchange capacity, and added back to the reactor [3]. During the residence time in the reactor charged natural organic matter species in the water phase undergoes ion exchange within the resin phase, thereby reducing the water phase concentration of this species. Because of the way in which this process operates, ion exchange resin particles have a distribution of both sizes and ages that represent the time they have been in the reactor without undergoing regeneration. This is a two-scale problem because the macroscale conditions in the CMFR are effected by mass transport phenomena within the set of ion exchange particles.

The ion exchange particles are micro-porous, consisting of rigid solid particles with an internal, water-filled pore structure. Species within the bulk aqueous phase can diffuse within the pore structure and interact with the solid surfaces within the resin via an ion exchange mechanism. This process thus involves two length scales, the macroscale of the reactor, which in this case is well mixed, and the microscale, which is the length scale of the individual resin particles. Diffusion is the dominant transport mechanism within the ion exchange particles, which are nearly spherical in shape. Like all mass transfer processes, mechanistic description of this ion exchange process requires consideration of the thermodynamic equilibrium state and the rate of approach to that state.

Previous work has modeled this ion exchange problem using a two-scale approach [4] consisting of a linear equilibrium relationship between the aqueous phase concentration and the solid phase concentration, a set of spherically symmetric microscale diffusion equations to describe the rate of ion exchange, and a macroscale ordinary differential equation to represent the overall effect of ion exchange from all particles on the aqueous phase concentration exciting the treatment process. Due to the nature of the CMFR, resin particles are not of a common age, and a residence time distribution (RTD) has to be introduced to describe the time different size particles have resided in the CMFR system. In order to simulate this two-scale model, Monte-Carlo schemes have been applied to sample particles of residence time, resulting in large systems of diffusion equations that must be solved simultaneously. Given the computational expense of this approach, it seems worthwhile to consider the development of an effective model that can represent the complexity of the real system without the expense of the Monte Carlo algorithm.

The two-scale Monte Carlo model for ion exchange has been approximated using a higher order Galerkin finite element method in space and a backward difference formula (BDF) method in time [4]. While efficient higher order BDF methods are well established, the Monte Carlo algorithm complicates the use of these higher order methods because the integration history needed for higher order is not available for new particles added to the system, effectively requiring a frequent restart of the integrator. Because of this, low-order BDF methods have been used for this problem. Therefore, the efficiency of the numerical approximation methods used for this ion exchange problem also appears to be fertile ground for gaining efficiency in the solution of this problem.

Recent work to develop integral equation based Krylov deferred correction (KDC) methods [17-19] accelerated by fast elliptic equation solvers [7,8,10,12-14] seems to be a potential avenue for gaining solution efficiency for this problem. In such approaches, the temporal direction is first discretized and the decoupled elliptic equations can then be solved with a fast elliptic solver. We further notice that the diffusion equation is stiff but linear, while the nonlinear macroscale ODE is non-stiff, so a semi-implicit marching scheme could be applied to the macroscale ODE model to provide boundary conditions for the microscale diffusion equations.

The overall goal of this work is to advance the efficiency of modeling multiscale ion exchange processes. The specific objectives are: (1) to develop an effective equation approach to the multiscale problem that obviates the need for Monte Carlo simulation; (2) to formulate a new numerical approximation method for this problem based upon evolving KDC-fast elliptic solver methods; (3) to evaluate the accuracy and efficiency of the solution methods resulting from changes in both the algorithm and approximation methods compared to extant approaches; and (4) to consider ways in which the evolving numerical approximation algorithm can be further improved for both this application and other potential applications.

This work is organized as follows. In §2, we present the classical model in which a set of microscopic diffusion equations are coupled to a macroscale ordinary differential equation and derive a new age-averaged model by averaging the resident time for the microscale models. In §3, we discuss the finite element based numerical approximation technique as well as a semi-implicit KDC method accelerated by a fast elliptic equation solver. Finally in § 4, numerical results are presented to compare the original two-scale model with the age-averaged model and to compare the standard FEM-based approximation scheme with a semi-implicit KDC approach.

2. Modeling Dissolved Organic Carbon Removal Process

Similar to most existing results in simulating the CMFR system, we assume that all ion exchange resin particles are spherical and homogeneous, although of varying radius and age. This assumption admits symmetry of the solution and a resulting reduction in spatial dimensionality. We also assume the dominant mechanism of transport within the resin particles is pore diffusion, whereby solute molecules diffuse in a Fickian manner through the water-filled pores and are in a state of linear local equilibrium with the solid phase. These assumptions have been used in prior work on this problem and proven to be reasonably accurate representations of the real system through model verification with experimental data [4].

2.1. Two-Scale Model

Unlike most similar mass transfer models in which a uniform particle size for the solid phase is assumed, we follow research results from [21,25] and add multiple particle size-classes, which more accurately represent the actual conditions present in the system. We denote the total number of such classes by N_{size} and assume the size distribution of the resin particles is time-independent [4]. Also, due to the flow in the CMFR system, each ion exchange resin particle is resident in the CMFR for a varying length of time, i.e., new resin particles come into the system continuously, simultaneously replacing an equal portion of the resident resin particles. Therefore, a residence time distribution (RTD) can be introduced to describe the “age” of each particle size class in the CMFR. We refer to the discretized total number of particle age-classes as N_{age}, which approximates the RTD.

2.1.1. Microscale Model—At the scale of an individual resin particle, which we will refer to as the microscale, we model transport as spherical diffusion through a homogeneous, symmetric particle through the following closed conservation of mass equation written in terms of the water-phase solute concentration c in the pore fluid as

$$\begin{cases} \left(1+\frac{(1-\epsilon_p)\rho_s}{\epsilon_p}\frac{\partial q}{\partial c}\right)\frac{\partial c}{\partial t}=\frac{D_{p,e}}{r^2}\frac{\partial}{\partial r}\left(r^2\frac{\partial c}{\partial r}\right) \\ c\,(t=0,r)=0 \\ \left.\frac{\partial c}{\partial r}\right|_{r=0}=0, t>0 \\ c(t>0, r=R)=C \end{cases}$$

where q is the solute mass fraction of the solid phase, which is a linear function of c, ϵp is the resin porosity, t is time, ρ_s is the solid phase density, $D_{p,e}$ is the effective pore diffusion coefficient, r is the radial distance from the center of the resin particle, R is the resin particle radius, and C is the solute concentration in the bulk fluid within the CMFR. We further assume that ϵ_p and ρ_s are constants and $D_{p,e}$ is independent of the solute concentration.

As in [4], we assume a linear relation between the solute concentration c in the pore fluid and the solute concentration q on the solid phase, which has been validated by experiments, and denote the linear factor by K_D, where $q = K_D c$. The microscale model is then given by

$$\begin{cases} \left(1+\frac{(1-\epsilon_p)\rho_s K_D}{\epsilon_p}\right)\frac{\partial c}{\partial t}=\frac{D_{p,e}}{r^2}\frac{\partial}{\partial r}\left(r^2\frac{\partial c}{\partial r}\right) \\ c\,(t=0,r)=0 \\ \left.\frac{\partial c}{\partial r}\right|_{r=0}=0, t>0 \\ c(t>0, r=R)=C. \end{cases} \tag{1}$$

Note that the solute concentration C in the CMFR is unknown in this microscale system. In order to complete the model, an equation for C at the macroscale will be developed in next section.

The equation system in (1) is for each specific particle size and age, therefore in the numerical simulation, $N_{size} \times N_{age}$ diffusion systems need to be solved at each time step, which is the most time consuming part of the numerical simulation.

2.1.2. Macroscale Model

—The macroscale portion of the model is a conservation of mass equation for a CMFR, which consists of mass entering the system in the water phase, mass exciting the system in the water phase, and mass transfer from the water phase to the ion exchange resin. Under the conditions of a constant volume of fluid V in the CMFR, the macroscale model is

$$\begin{cases} V\frac{dC}{dt}=Q(C_0-C)-M^{a-s}, \\ C(t=0)=C_0, \end{cases} \tag{2}$$

where V is the volume of the water phase in the reactor, Q is the volumetric flow rate, C_0 is the influent solute concentration, C is the effluent solute concentration from the reactor equal to the solute concentration in the bulk fluid phase, and M^{a-s} is the total interphase mass exchange of solute from the aqueous phase to the resin phase, which can be determined by the microscale model using

$$M^{a-s}=\frac{m_s}{(1-\epsilon_p)\rho_s R}3F,$$

where F is the microscale mass flux and m_s is the total mass of solids in the system defined as

$$m_s=C_R\rho_a V.$$

Here C_R is the volume of resin normalized by the volume of the water in the reactor, the resin is assumed to be incompressible, and $\rho_a = (1 - \epsilon_p)\rho_s$ is the bulk density of the resin. For a system with the same size and age particles, the flux into the particle is defined by

$$F=\epsilon_p D_{p,e}\left.\frac{\partial c}{\partial r}\right|_{r=R}.$$

This equation shows how the macroscale model couples with the microscale system. For a system with multiple sizes and ages of resin particles, M^{a-s} can be defined as the integral of flux with respect to particle sizes and ages as in

$$M^{a-s}=\frac{3\epsilon_p D_{p,e} m_s}{\rho_a}\int_{Rmin}^{Rmax}\int_{tmin}^{tmax}\frac{1}{R}\left.\frac{\partial c}{\partial r}\right|_{r=R} g(t_a)h(R)dt_a dR$$

where $g(t_a)$ is the particle age probability density function, and $h(R)$ is the particle size probability density function.

2.1.3. Two-Scale Model—Combining the micro- and macro-scale systems, the two-scale model for the ion exchange process is summarized by Eqs. (3-4) as follows. At microscale, for each resin particle size the retarded diffusion equation model is

$$\begin{cases} R_f\frac{\partial c}{\partial t}=\frac{D_{p,e}}{r^2}\frac{\partial}{\partial r}\left(r^2\frac{\partial c}{\partial r}\right), \\ c(t=0,r)=0, \\ \left.\frac{\partial c}{\partial r}\right|_{r=0}=0, t>0, \\ c(t>0,r=R)=C \end{cases} \tag{3}$$

where the retardation factor is

$$R_f=1+\frac{\rho_a K_D}{\epsilon_p}.$$

At macroscale, Eq. (2) can be rewritten as follows:

$$\begin{cases} \frac{dC}{dt}=\frac{Q}{V}(C_0-C)-M^{a-s}/V, \\ C(t=0)=C_0. \end{cases} \tag{4}$$

For a batch system with no inflow or outflow, and a constant age of resin particles, Eq. (4) can be written as follows:

$$\begin{cases} \frac{dC}{dt} = -M^{a-s}/V, \\ C(t=0) = C_0. \end{cases} \tag{5}$$

2.2. Age-Averaged Model

In order to simulate the two-scale model with the traditional algorithm, a diffusion equation (3) must be solved at every time step for each particle size and age sampled by the Monte-Carlo method. The solution of the $N_{size} \times N_{age}$ diffusion equations is the most time consuming part of the numerical simulation. In this section, instead of using the Monte-Carlo approach to approximate the RTD (age), we derive a new age-averaged model, by introducing a new unknown variable

$$c_s(t,r) = \sum_{\text{all size } s \text{ particles}} c_{s,a}(t,r) \tag{6}$$

where $c_{s,a}$ is the solute concentration in the original two-scale model for a specific particle of size s and age a, and the summation is for all particles of the same size s (two particles may have the same size and age).

To derive the corresponding microscale equation for $c_s(t, r)$, we consider $c_s(t + \Delta t, r) - c_s(t, r)$, which can be computed as

$$c_s(t+\Delta t,r) - c_s(t,r) = \sum_{\text{staying}} (c_{s,a}(t+\Delta t,r) - c_{s,a}(t,r)) - \sum_{\text{outgoing}} c_{s,a}(t_i,r) + \sum_{\text{incoming}} c_{s,a}(t_i,r), \quad t_i \in [t, t+\Delta t]$$

where “staying” particles represent the particles that are in the system from time t to $t + \Delta t$, “outgoing” and “incoming” particles are those particles leaving and entering the CMFR in the time interval $[t, t + \Delta t]$, respectively. Further notice that for the “incoming” particles, $c_{s,a}(t_i, r) = 0$ initially and Σoutgoing $c_{s,a}(t_i, r)$ can be determined by the outgoing flow rate and the current $c_s(t, r)$ as in

$$\sum_{\text{outgoing}} c_{s,a}(t_i,r) = kc_s(t,r)\Delta t$$

where k is determined by the outgoing flow rate in the CFMR system. Therefore,

$$\frac{c_s(t+\Delta t,r) - c_s(t,r)}{\Delta t} = \sum_{\text{staying}} \left(\frac{c_{s,a}(t+\Delta t,r) - c_{s,a}(t,r)}{\Delta t} \right) - kc_s(t).$$

As $c_{s,a}(t, r)$ satisfies the diffusion equation, letting $\Delta t \rightarrow 0$, we can derive the differential equation for $c_s(t, r)$ and the resulting microscale system in the averaged model becomes

$$\begin{cases} R_f \frac{\partial c_s(t,r)}{\partial t} = \frac{D_{p,e}}{r^2}\frac{\partial}{\partial r}\left(r^2 \frac{\partial c_s(t,r)}{\partial r}\right) - kR_f c_s(t,r), \\ c_s(t=0, r)=0, \\ \left.\frac{\partial c_s(t,r)}{\partial r}\right|_{r=0} = 0, t>0, \\ c_s(t>0, r=R)=n \cdot C \end{cases}$$

where n is the total number of particles of size s and the initial and boundary conditions are determined by studying the summation in Eq. (6). Normalize the variable c_s by $\tilde{c}_s(t, r) = c_s(t, r)/n$, we derive the age-averaged equation in

$$\begin{cases} R_f \frac{\partial \tilde{c}_s(t,r)}{\partial t} = \frac{D_{p,e}}{r^2}\frac{\partial}{\partial r}\left(r^2 \frac{\partial \tilde{c}_s(t,r)}{\partial r}\right) - kR_f \tilde{c}_s(t,r), \\ \tilde{c}_s(t=0, r)=0, \\ \left.\frac{\partial \tilde{c}_s(t,r)}{\partial r}\right|_{r=0} = 0, t>0, \\ \tilde{c}_s(t>0, r=R)=C. \end{cases}$$

To simplify the notation, we slightly abuse our notation and use c_s to represent the normalized $\tilde{c}_s$, and summarize the age-averaged model as follows at the microscale

$$\begin{cases} R_f \frac{\partial c_s(t,r)}{\partial t} = \frac{D_{p,e}}{r^2}\frac{\partial}{\partial r}\left(r^2 \frac{\partial c_s(t,r)}{\partial r}\right) - kR_f c_s(t,r), \\ c_s(t=0, r)=0, \\ \left.\frac{\partial c_s(t,r)}{\partial r}\right|_{r=0} = 0, t>0, \\ c_s(t>0, r=R)=C, \end{cases} \tag{7}$$

and at the macroscale

$$\begin{cases} \frac{dC}{dt} = \frac{Q}{V}(C_0 - C) - \frac{M^{a-s}}{V}, \\ C(t=0)=C_0. \end{cases} \tag{8}$$

Compared with the original two-scale model, the microscale system in the age-averaged model becomes a system of microscale diffusion-reaction equations, and the coefficient for each reaction term can be measured or controlled by the regeneration rate of the ion exchange resin in the CMFR system. Because, we have a well-mixed system in which the size distribution is constant with time, k will be constant for all particle sizes. An immediate advantage of the AAM is that sampling of different ages is no longer necessary, hence the numerical simulations are greatly simplified.

3. Numerical Algorithms

There exist many numerical techniques to approximate the solution of systems of differential equation initial value problems [1,5,11,15,16,23]. In this section, we discuss two types of numerical methods for approximating the solution of the original two-scale model and new age-averaged model, including (1) a finite element method (FEM) based scheme; and (2) a new Krylov-deferred-correction (KDC) method accelerated by a fast elliptic equation solver. These approaches are discussed in turn in the sections that follow.

3.1. Finite Element Method

In the first numerical scheme, we used the Galerkin finite element method (FEM) with cubic Lagrange polynomials as basis and test functions for the approximation in the spatial direction and discretized the spatial nodes to yield equal volume cubic elements. Gaussian quadrature was used to integrate the cubic Lagrange polynomials and nodes were spaced equidistant within each element.

The resulting ordinary differential equation (ODE) system was solved using existing initial value ODE solvers. In our matlab implementation, $ode15s$ was used for time integration with the AAM. However, for the traditional Monte-Carlo algorithm, $ode15s$ was inefficient because the history of the ODE system was reinitialized whenever a new particle was added to the system, which required that the integrator be restarted. Because of this, it was found that a backward Euler approach was more efficient for the Monte Carlo algorithm than a higher order approach. All results for the Monte Carlo method with a FEM solution approximation in space thus used backward Euler time integration. The FEM method results in a set of linear equaitions that must be solved at each time step. Ordering of the equations allowed this system to be formed as a banded system, which was efficiently solved using a single lower-upper-decomposition factoring, followed by a sparse back substitution at each time step. The linear algebra portion of the solution scale linearly with the number of particles in the system. We refer interested readers to [4] for the application of the FEM to the original two-scale model in which a Monte-Carlo algorithm was used to approximate the RTD of the resin particles. The FEM solution used in this work is relatively mature, efficiently implemented, uses higher order methods in space and variable element spacing, but is restricted because of the Monte-Carlo algorithm to a low-order method in time.

3.2. Krylov Deferred Correction Method

The KDC method was first introduced in [17] in which it was analytically shown that for linear problems, the spectral deferred correction (SDC) method introduced in [9] is equivalent to solving a preconditioned form of a collocation formulation resulting from a Neumann series expansion. Instead of simply accepting the Neumann series result, in the KDC scheme the collocation system is preconditioned by the SDC method, and is solved efficiently using a Newton-Krylov(NK) method to accelerate the convergence and avoid the divergence of SDC methods for certain kinds of equations. Further, a Jacobian-Free NK (JFNK) scheme [20] is used to avoid the costly evaluation of the Jacobian matrix of the preconditioned system.

As the KDC method is new and evolving, in this section we briefly explain how the KDC method works for a general parabolic type partial differential equation (PDE) system of the form

$$L(u_t, u, u_x, u_{xx})=0 \tag{9}$$

where $u = u(x, t)$ and proper initial and boundary conditions are given. Interested readers are referred to [19] for a detailed description of the KDC method for approximating the solution of PDE's.

To march from t_0 to $t_0 + \Delta t$ in the KDC scheme, instead of using a traditional discretization scheme based on the differential form of the equation, we first introduce $U = u_t$ as the new unknown, and discretize the PDE in the temporal direction using p Gaussian quadrature nodes $\vec{t} = [t_1, t_2, \cdots, t_p]^T$.

The resulting discretized system becomes a coupled elliptic equation system

$$L\left(U, u_0+\Delta tS\otimes U, \frac{d}{dx}(u_0+\Delta tS\otimes U), \frac{d^2}{dx^2}(u_0+\Delta tS\otimes U)\right)=0 \tag{10}$$

where ΔtS is a matrix mapping the function values $\{U(x, t_m), m = 1,\cdots, p\}$ at the Gaussian nodes $\tilde{t}$ to their temporal integral $\int U(x, t)dt$ using spectral integration as discussed in [9], ⊗ denotes the component-wise tensor product of the spectral integration matrix (ΔtS is applied to the vector $\{U(x, t_m)\}_{m=1}^{p}$ for each fixed x), and $u_0 + \Delta tS \otimes U$ represents the matrix form of the spectrally accurate approximation of the solution $u(x)$ in one big time step. In this paper, we symbolically denote this collocation formulation in Eq. (10) as $H(U) = 0$. Notice that although this formulation has excellent numerical properties in accuracy and stability, its direct solution is in general computationally expensive as the unknowns are coupled at all times (the solution $U(x, t_m)$ depends on the unknowns $U(x, t_i)$ for $i = 1, \cdots, p$), while in the traditional backward differentiation formula (BDF) or many Runge-Kutta based methods, the solution $U(x, t_m)$ only depends on the values $U(x, t_i)$ at previous times $i = 1, \cdots, m$.

Instead of solving the collocation formulation in Eq. (10) directly in the KDC method, we assume a provisional solution $\tilde{U}$ derived by the low-order BDF or Runge-Kutta method, and define the equation for the error $\delta = U–\tilde{U}$ by

$$L\left[\tilde{U}+\delta, u_0+\Delta tS\otimes(\tilde{U}+\delta), \frac{d}{dx}\left(u_0+\Delta tS\otimes(\tilde{U}+\delta)\right), \frac{d^2}{dx^2}\left(u_0+\Delta tS\otimes(\tilde{U}+\delta)\right)\right]=0 \tag{11}$$

To find an approximate solution of the error δ which will be denoted by $\tilde{\delta}$, we can apply the BDF or Runge-Kutta method to Eq. (11), which is equivalent to solving

$$L\left[\tilde{U}+\tilde{\delta}, u_0+\Delta tS\,\tilde{U}+\Delta t\,\tilde{S}\tilde{\delta}, \frac{d}{dx}\left(u_0+\Delta tS\,\tilde{U}+\Delta t\,\tilde{S}\tilde{\delta}\right), \frac{d^2}{dx^2}\left(u_0+\Delta tS\,\tilde{U}+\Delta t\,\tilde{S}\tilde{\delta}\right)\right]=0 \tag{12}$$

where $\tilde{S}$ is the corresponding lower triangular approximation of the spectral integration matrix S. In particular, the forward Euler method is equivalent to the rectangle rule using the left end point (derivative information at left end point) and the backward Euler method is the rectangle rule using the right end point (derivative information at right end point). Notice that in Eq. (12), the unknowns $\tilde{\delta}(x, t_m)$ at different times are "decoupled" such that $\tilde{\delta}(x, t_m)$ only depends on $\tilde{\delta}(x, t_i)$ at previous times $i = 1, \cdots, m$ as in traditional time marching schemes, and each decoupled elliptic equation can be solved efficiently using a fast elliptic equation solver.

In the original SDC method [9], a low-order approximate solution $\tilde{\delta}$ was added to the provisional solution $\tilde{U}$ to derive a better approximation of the solution U, and the updated $\tilde{U}$ was used to derive a new error equation. This iteration continued for a fixed number of times or when a prescribed accuracy tolerance was achieved. In [17], it was shown that for linear problems, this SDC procedure is equivalent to a preconditioned Neumann series expansion in which the preconditioner is the lower order time stepping scheme. In [18], it was numerically shown that this Neumann series expansion is divergent for many differential algebraic equation systems. To accelerate the convergence and avoid the divergence of the SDC method, in [18], Eq. (12) was considered as an implicit function $\tilde{\delta} = \tilde{H}(\tilde{U})$. Since the Jacobian matrix of $\tilde{H}$ is closer to $-I$, the Newton-Krylov method can be adapted and applied directly to find the zero of the implicit function, which also solves the original collocation formulation in Eq. (10). This Newton-Krylov method for the SDC preconditioned system in Eq. (12) is referred to as the Krylov deferred correction (KDC) method.

KDC methods can be coupled with many existing low order time stepping schemes. It would also be possible to combine the KDC temporal solution approach with the FEM method used in this work. In this paper, the KDC scheme is compared with the FEM approach which was presented in previous work [4]. Further efficiency acceleration of the FEM using KDC and other techniques are not considered in this work.

3.3. Semi-Implicit KDC Method

The application of the KDC method to the two-scale model using both the extant Monte Carlo algorithm and the new AAM is straightforward. For the macroscale ODE system, introducing $U = dC/dt$ as the new unknown, a Picard type integral equation formulation results of the form given by

$$U=\frac{Q}{V}\left[C_0-\left(C_{0,m}+\int_0^t U(\tau)d\tau\right)\right]-\frac{M^{a-s}}{V},$$

where M^{a-s} is determined by solving the system of microscale diffusion equations using either the Monte Carlo or the AAM algorithm. Assuming a provisional solution $\tilde{U}$ is available, we can define the error δ using $U = \tilde{U} + \delta$, and the Picard equation for the error is given by

$$\tilde{U}+\delta=\frac{Q}{V}\left[C_0-\left(C_{0,m}+\int_0^t\left(\tilde{U}(\tau)+\delta(\tau)\right)d\tau\right)\right]-\frac{M^{a-s}}{V}. \tag{13}$$

Similarly, for the diffusion equation (Monte Carlo algorithm) or the diffusion-reaction equation (AAM), we can introduce $Y(t, r) = \partial c(t, r)/\partial t$ as the new unknown, where c is either $c_{s,a}$ for each sampled size and age particle in the Monte Carlo method, or c_s in AAM, and derive a Picard integral equation and corresponding error equation for Y. Specifically, for the Monte Carlo method, the Picard type equation for each diffusion equation of the form

$$rR_f\frac{\partial c}{\partial t}=2D_{p,e}\frac{\partial c}{\partial r}+rD_{p,e}\frac{\partial^2 c}{\partial r^2}$$

is given by

$$r\frac{R_f}{D_{p,e}}Y-2\frac{d}{dr}\int_0^t Y(\tau,r)d\tau-r\frac{d^2}{dr^2}\int_0^t Y(\tau,r)d\tau=2\frac{d}{dr}c_0+r\frac{d^2}{dr^2}c_0.$$

Assuming a provisional solution $\tilde{Y}$ is available, the error equation for the error $\gamma(t, r) = Y(t, r) - \tilde{Y}(t, r)$ becomes

$$r\frac{R_f}{D_{p,e}}(\tilde{Y}+\gamma)-2\frac{d}{dr}\int_0^t\left(\tilde{Y}(\tau,r)+\gamma(\tau,r)\right)d\tau-r\frac{d^2}{dr^2}\int_0^t\left(\tilde{Y}(\tau,r)+\gamma(\tau,r)\right)d\tau=2\frac{d}{dr}c_0+r\frac{d^2}{dr^2}c_0. \tag{14}$$

The approach for the AAM is nearly identical, except for the reaction term, so we will neglect these details without loss of clarity or completeness.

In the original KDC methods [18,19], for a given error equation, an explicit low-order scheme (e.g., forward Euler method) was applied if the system was non-stiff or mildly stiff, and an implicit low-order scheme (e.g., backward Euler method) was used to approximate the error for stiff systems.

In this section, to further improve the efficiency of the KDC methods, we notice that the diffusion equation for γ is stiff but linear, and the macroscale error equation for δ is non-stiff. Therefore, a semi-implicit KDC scheme can be used in which an implicit scheme is applied to the microscale diffusion system and an explicit technique is applied to the nonstiff macroscale ODE system.

In order to solve the error equations (13 and 14) when marching from t_m to t_{m+1} in the semi-implicit KDC (SI-KDC) scheme, we first apply an explicit low-order time stepping scheme to the discretized macroscale equation. Application of the forward Euler method yields the discretized system given by

$$\tilde{U}_{m+1}+\tilde{\delta}_{m+1}=\frac{Q}{V}\left[C_0-\left(C_{0,m}+\Delta tS\otimes\tilde{U}+\sum_{l=1}^{m+1}\Delta t_l\tilde{\delta}_{l-1}\right)\right]-\left(\frac{M^{a-s}}{V}\right)_m \tag{15}$$

where $\Delta t_{l+1} = t_{l+1} - t_l$ and $\delta_0 = 0$. Notice that no data at time t_{m+1} is required on the right hand side of the equation. We further denote Eq. (15) as an implicit function for $\tilde{\delta}$ whose explicit form is given by

$$\tilde{\delta}=\tilde{H}_{macro}(\tilde{U},\tilde{Y})=\left(1+\frac{Q}{V}\Delta t\tilde{S}_E\right)^{-1}\left[\frac{Q}{V}\left(C_0-C_{0,m}-\Delta tS\,\tilde{U}\right)-\tilde{U}-\left(\frac{M^{a-s}}{V}\right)_m\right] \tag{16}$$

where $\tilde{S}_E$ is the matrix form of the lower-triangular approximation of the spectral integration matrix S, which is equivalent to an explicit low-order time stepping scheme, and the dependence on $\tilde{Y}$ is implicitly expressed in M^{a-s}/V.

Once $\tilde{\delta}_{m+1}$ is available, we can explicitly derive the boundary condition for the microscale model at time t_{m+1}. To march the diffusion type error equation (14) from t_m to t_{m+1} using a low-order method, as the equation is stiff, an implicit scheme has to be applied in general for efficiency considerations (as much larger time stepsize can be used). In our current implementation, the backward Euler method is used, and the discretized system for $\tilde{\gamma}_{m+1}$ becomes

$$r\frac{R_f}{D_{p,e}}Y-2\frac{d}{dr}\left(\Delta tS+\sum_{l=1}^{m+1}\Delta t\tilde{\gamma}_l\right)-r\frac{d^2}{dr^2}\left(\Delta tS+\sum_{l=1}^{m+1}\Delta t\tilde{\gamma}_l\right)=2\frac{d}{dr}c_0+r\frac{d^2}{dr^2}c_0, \tag{17}$$

which can written as an implicit method for $\tilde{\gamma}$ whose explicit form is given by

$$\tilde{\gamma}=\tilde{H}_{micro}(\tilde{U},\tilde{Y})=\left(r\frac{R_f}{D_{p,e}}-2\frac{d}{dr}\Delta t\tilde{S}_I-r\frac{d^2}{dr^2}\Delta t\tilde{S}_I\right)^{-1}\left(\frac{d^2}{dr^2}r(c_0+\Delta tS\,\tilde{Y})+2\frac{d}{dr}(c_0+\Delta tS\,\tilde{Y})-r\frac{R_f}{D_{p,e}}\,\tilde{Y}\right) \tag{18}$$

where $\tilde{S}_I$ is the corresponding lower triangular approximation of the spectral integration matrix S, and the dependency on $\tilde{U}$ is implicitly expressed in the boundary conditions. Notice that to find $\tilde{\gamma}_{m+1}(r)$, a linear elliptic equation of the form

$$a^2\tilde{\gamma}_{m+1}(r) - \nabla^2\tilde{\gamma}_{m+1}(r) = f(r)$$

must be solved, where all the known quantities are collected in *f*(*r*). This will be discussed in the next section.

Since the zero of the preconditioned implicit microscale and macroscale system given by

$$\begin{cases} 0=\tilde{H}_{macro}(\tilde{U},\tilde{Y})=\tilde{\delta}, \\ 0=\tilde{H}_{micro}(\tilde{U},\tilde{Y})=\tilde{\gamma} \end{cases} \tag{19}$$

also satisfies the original collocation formulation symbolically denoted as

$$\begin{cases} 0=H_{macro}(U,Y), \\ 0=H_{micro}(U,Y) \end{cases} \tag{20}$$

for both the Monte Carlo method and AAM, the Jacobian matrix of the preconditioned system (19) is closer to the identity matrix than the original formulation (20), the JFNK method can be applied directly to solve the preconditioned system (19), and each function evaluation is simply one low-order time stepping approximation of the errors $\tilde{\delta}$ and $\tilde{\gamma}$.

It is also possible to further improve the efficiency of the algorithm by only applying the Newton-Krylov methods to $\tilde{\delta} = \tilde{H}_{macro}(\tilde{U})$, and consider the microscale equations as implicit functions of $\tilde{\delta}$. The advantage of doing so is that the number of operations and required storage can be greatly reduced in the Krylov iterations.

Finally, we note that there is a discontinuity in the solution of the diffusion equation or the diffusion reaction equation: when $t = 0$, the boundary condition at $r = R$ is given by $C \neq 0$, while the solution inside the resin particle $c(t = 0, r) = 0$. Therefore in our numerical simulation, we apply the second-order Crank-Nicolson method for the initial several time steps with very small step-sizes, and start the higher order SI-KDC solver once the solution becomes reasonably smooth. This will be further discussed in Sec. 4.

3.4. Fast Elliptic Solver

When the microscale diffusion or diffusion-reaction equation is discretized using a low-order implicit time stepping scheme (e.g., the backward Euler method), the resulting system becomes a Poisson type equation in the form

$$a^2u - \nabla^2u = k^2u - \frac{1}{r^2}\frac{\partial}{\partial r}\left(r^2\frac{\partial u}{\partial r}\right) = f(r) \tag{21}$$

where *f*(*r*) is a given function. This equation is often referred to as the modified Helmholtz equation in computational fluid dynamics, or the linearized Poisson-Boltzmann equation when simulating the electrostatics in biomolecular systems. Existing numerical schemes for this equation include finite difference, finite element, and integral equation methods. In particular, accurate and efficient numerical methods based on integral equation formulations accelerated by fast algorithms are discussed in [7,8,10,12-14]. In this paper, we present the Chebyshev spectral integration method for the special spherical geometry, and discuss a numerical scheme for the efficient solution of the scaled equation

$$cru-2u'-ru''=f(r). \tag{22}$$

When the resin particles are of complex geometry, we refer interested readers to [7,10,14] for several integral equation methods accelerated by the new version of Fast Multipole Methods (FMM).

In the Chebyshev spectral integration method, unlike traditional spectral methods, we set the unknowns as the coefficients of the Chebyshev expansion of u'' as in

$$u''(r)=\sum_{m=0} a_m T_m(r)$$

where T_m is the Chebyshev polynomial of degree m defined as

$$T_m(r)=\cos(m\cos^{-1}r),$$

and we assume the Chebyshev expansion of the function $f(r)$ is given by

$$f(r)=\sum_{m=0} b_m T_m(r).$$

The advantage of studying the Chebyshev expansion of u'' instead of the expansion for u is that the spectral integration matrix, which maps the coefficients of u'' to those of u', has a tridiagonal form as discussed in [12], and the resulting linear system for $\{a_m\}$ forms a hepta-diagonal system, which can be solved using approximately $O(P)$ operations where P terms are used in the expansion. Also, the spectral integration schemes are more accurate and stable than the corresponding spectral differentiation based schemes, as discussed in [6,9,12].

4. Simulation Results

In this section, we present numerical simulation results using the FEM and SI-KDC schemes for both the original Monte Carlo method and the new AAM for the two-scale ion exchange application. Our simulations were performed on a laptop with an Intel 2GHz CPU and 1GB of RAM.

4.1. Accuracy and Efficiency Comparisons

To study the accuracy and efficiency of the FEM and KDC methods, we applied the methods to a diffusion equation system

$$\frac{\partial c}{\partial t}=\frac{D}{R_f}\left(\frac{\partial^2 c}{\partial r^2}+\frac{2}{r}\frac{\partial c}{\partial r}\right)$$

with fixed boundary conditions. Introducing the new unknown $u(t, r) = c(t, r) \cdot r$, the equation for u becomes

$$\frac{\partial u}{\partial t}=\frac{D}{R_f}\frac{\partial^2 u}{\partial r^2}$$

with initial and boundary conditions

$$\begin{cases} u(t, r=0)=0, \\ u(t, r=R)=RC_0, \\ u(t=0, r)=r\, f(r), 0<r<R \end{cases}$$

where C_0 is the constant concentration at the surface of the sphere. Notice that at $t = 0$, C_0 is not necessarily the same as $f(R)$. This discontinuity in the initial/boundary values makes the numerical simulation difficult when using approximation schemes requiring smoothness properties of the solution. In this example, as the pseudo-spectral formulation based KDC schemes are not advantageous for solutions with such a discontinuity, so we first use a low-order method to march the equation from $t = 0$ to $t = 0.01$. Once the solution becomes “smooth,” the KDC approach is applied. There exist many numerical schemes for dealing with the sharp initial solution, and our approach was intended to provide an approach that contributed negligibly to the error in the solution, but it is not an optimal approach. For example, the analytical form of this sharp solution can be extracted using a Laplace transform and method of images, and the KDC technique could then be applied to the remaining smooth part of the solution.

In Fig. 2, we first compare the accuracy of the FEM and KDC schemes. In the FEM based scheme, cubic Lagrange polynomials are used as basis functions for the Galerkin formulation and discretization is accomplished using 32 spatial nodes, which were regularly spaced within 10 equivalent volume elements. In the KDC method, the spatial elliptic equation was solved using the Chebyshev spectral integration method with 32 Chebyshev nodes and the solution was further accelerated by using the fast Fourier transform (FFT). For the temporal direction, seven Radau IIa nodes were used so the temporal order was approximately 13. In both simulations, we marched from $t = 0.01$ (so the analytical solution is reasonably smooth) to $t_{final} = 1$ with $\Delta t = 0.1$ (except for the last step), and use the exact solution to derive the initial and boundary values.

From the numerical simulations, it can be seen that results from both the KDC and FEM are close to the analytic solution. However, the results from the KDC method are more accurate than those from FEM, which is not surprising due to the very high-order of the KDC scheme. As for the efficiency of the numerical schemes, in order to acquire 5 to 9 digits accuracy in the KDC scheme, the number of required function evaluations (each elliptic equation solve = one “function evaluation”) is in the range of 10 and 30. While for the FEM, over 300 function evaluations are required to obtain 6 to 7 digits of accuracy.

Higher order (in time) KDC methods may not be advantageous for “non-smooth” solutions. For this test problem, as the given initial condition is discontinuous in spatial and temporal directions at ($r = 1$, $t = 0$), a Crank-Nicolson method in time was applied for the first few steps, and the higher order KDC method was used once the solution became reasonably smooth. In Fig. 3, we compare the smoothness of the solution at $t = 0.0001$, $t = 0.001$, and $t = 0.01$. Our numerical experiments show that using 32 spatial nodes for the interval [0, 1] and 7 temporal nodes for each marching step with step-size 0.069, the KDC method can sufficiently resolve the solution in the time interval [0.01, 0.7]. However such settings can not accurately resolve the solution for $t < 0.01$.

Due to the “non-smoothness” of the solution and current non-adaptive implementation of the KDC scheme, our numerical experiments show that compared with FEM, KDC methods are less efficient when marching from $t = 0.0001$ to $t = 0.01$ for the same accuracy requirement, while they become more efficient when marching from $t = 0.01$ to $t = 0.7$.

In Fig. 4, we compare the efficiency and accuracy of the FEM and KDC methods by plotting the CPU time versus error. To minimize random computer execution factors in the operating system, both methods were executed 100 times. For both methods, we used a low-order scheme to march from $t = 0$ to $t = 0.01$. Once the solution becomes reasonably smooth, the KDC scheme was used to march from $t = 0.01$ to $t = 0.7$ with fixed time step-size $\Delta t = 0.069$, while an adaptive strategy was applied in the FEM using matlab built-in ODE solvers. Our numerical results show that for the same accuracy requirement, the KDC scheme is more efficient than the FEM based method for this example. It is important to note the FEM method used an optimized variable order, variable time step size method, whereas the KDC method was a relatively crude fixed order, fixed step size algorithm. One could further improve the efficiency of the KDC scheme using optimal control parameters, including the number of nodal points in the spatial and temporal directions, error tolerance, and an adaptive strategy in step-size and order selection. Results along these directions will be reported in the future.

Our numerical experiments also reveal that higher order methods become more efficient for smooth solutions. In Fig. 5, we show how the accuracy of the KDC methods depends on the number of Radau IIa collocation nodes for different time step-sizes, by comparing the accuracy as a function of the number of elliptic equation solves. Note that instead of CPU time, we compare the number of function evaluations for varying numbers of Radau nodes since the CPU time for KDC methods is linearly related to the number of function evaluations. Our numerical results show that for a fixed number of Radau IIa nodes, smaller time step-size means better accuracy; and for the same accuracy requirement, higher order schemes are more efficient than low-order schemes, especially when very high precision is required.

In Fig. 6, we show the convergence of the KDC methods for different number of Radau IIa nodes and step-sizes. It can be seen that for the same step-size, using more node points will generate more accurate results, and for the same number of node points, the error decreases rapidly when using smaller step-sizes. Also, due to the large step-size used by the KDC schemes for higher accuracy requirements ($\Delta t \approx 0.5$ for 13 digits accuracy when using 5 Radau node points), we couldn’t obeserve the traditional convergence orders (when Δt is close to 0) in our numerical simulation.

4.2. Multiple Particle Size and Age System

In our second example, we consider a resin particle system with 5 different sizes $R = 0.07$, 0.09, 0.10, 0.11, and 0.13, and assume they are of the same age and there is no flow($Q = 0$) in the batch system. The corresponding microscale system for each particle is given by

$$\begin{cases} \frac{\partial c}{\partial t} = \frac{2}{r}\frac{D}{R_f}\frac{\partial c}{\partial r} + \frac{D}{R_f}\frac{\partial^2 c}{\partial r^2}, \\ c(r, t=0)=0, \\ \left.\frac{\partial c}{\partial r}\right|_{r=0} =0, \\ c(r=R)=C(t) \end{cases}$$

with dynamical boundary condition described by the macroscale model

$$\begin{cases} \frac{dC}{dt} = -M^{a-s}/V, \\ C(0) = C_0 = 1. \end{cases} \tag{23}$$

In the KDC method, we use 20 Radau IIa points in the temporal direction from $t_0 = 0.015$ to $t_{final} = 1.0$ with step-size $\Delta t = 0.0985$ and 32 Chebyshev nodes in the spatial direction in [0, R] for each particle. In Fig. 7, we compare the results from the KDC scheme to those from the FEM based method, which has been validated by experimental results in [4]. The KDC results match those from FEM and experiments.

To compare the efficiency of the SI-KDC and FEM methods for this example, we plot the CPU time of both methods as a function of the error defined as the difference between the numerical solution and a fine-mesh reference solution in Fig. 8. Our numerical results show that for the same accuracy, the SI-KDC method is more efficient, especially for higher accuracy requirements.

4.3. Age-Averaged Model

Finally in this section, we compare the numerical results from the original Monte Carlo algorithm and the AAM. To validate the AAM, we compare results using the FEM for the traditional Monte Carlo algorithm with the AAM. For the Monte Carlo algorithm, we used 20 different particle sizes and 80 different particle ages for each size particle. We further assume that the radii for particles follow a log-normal distribution with mean log(100.6)–0.5 and standard deviation 1. Settings for other parameters can be found from previous work in [4].

In Fig. 9(a), we show simulation results for both traditional Monte Carlo method and the AAM. In Fig. 9(b), we plot the error for both methods using a very fine mesh reference solution. We notice that due to the Monte-Carlo nature of traditional two-scale model simulations, which requires sampling of particle ages at each time marching step, randomness can be observed in the error of the Monte Carlo solution, while the error from AAM is much smoother and smaller. The Monte Carlo method requires more CPU time due to the solution of different age elliptic equation systems, while only one elliptic equation solve is required for each particle size in AAM as age sampling is no longer necessary. Our numerical experiments show that for this example, the Monte Carlo method needed 1525.6 sec, while AAM required 74.3 sec in CPU time to obtain a much more accurate solution.

To compare the FEM with SI-KDC scheme for the age-averaged model, in Fig. 10 we show the computed concentration as a function of time in (a) and the CPU times for different accuracy requirements in (b). In the SI-KDC scheme, 32 Chebyshev nodes were used in the spatial direction and 30 Radau IIa nodes were used from $t = 0.01$ to $t_{final} = 10.0$ with $\Delta t = 0.999$. As mentioned in previous sections, the second-order Crank-Nicolson method was used from $t = 0$ to $t = 0.01$, and when the solution becomes reasonably smooth, the SI-KDC method was applied thereafter. The simulation results are similar for both methods, while for the same accuracy requirements, the SI-KDC is more efficient.

5. Summary

The results of this work detail the derivation and validation of an age-averaged model for the solution of a two-scale ion exchange problem, which is shown to be exact in form, thus much more accurate and computationally less expensive than the traditional Monte Carlo solution method. We also advance a semi-implicit Krylov-deferred correction method coupled with a fast elliptic solver to approximate the large coupled system of differential equations, and we show that this method is much more efficient than the traditional finite element solution method with higher order time integration, especially for high accuracy solutions. The SI-KDC method did require a smooth initial condition to be efficient. Future work should be geared toward refining the SI-KDC method to result in a self-adaptive algorithm to vary the step size and order of the method in order accommodate less smooth solutions and to further improve computational efficiency.

Acknowledgments

The work of CTM was supported by National Science Foundation Grant ATM-0941235 and National Institute of Environmental Health Sciences Grant P42 ES05948. The work of JH was supported by NSF-0811130 and NSF-0905473. Part of the work was done when SB was a visiting member of the Institute for Mathematics and Applications (IMA) at the University of Minnesota. Their support is thankfully acknowledged.

References

1. Atkinson, K. An Introduction to Advanced Numerical Analysis. 2. John Wiley; 1989.
2. Boyer TH, Singer PC. Bench-scale testing of a magnetic ion exchange resin for removal of disinfection by-product precursors. Water Research 2005;39(7):1265–1276. [PubMed: 15862326]
3. Boyer TH, Singer PC. A pilot-scale evaluation of magnetic ion exchange treatment for removal of natural organic material and inorganic anions. Water Research 2006;40(15):2865–2876. [PubMed: 16844182]
4. Boyer TH, Miller CT, Singer PC. Modeling the removal of dissolved organic carbon by ion exchange in a completely mixed flow reactor. Water Research April;2008 42(8-9):1897–1906. [PubMed: 18082241]
5. Brenan, KE.; Campbell, SL.; Petzold, LR. Numerical Solution of Initial-Value Problems in Differential-Algebraic Equations. SIAM; Philadelphia: 1995.
6. Canuto, C.; Hussaini, MY.; Quarteroni, A.; Zang, TA. Spectral Methods in Fluid Dynamics. Springer-Verlag; 1988.
7. Cheng H, et al. A wideband fast multipole method for the Helmholtz equation in three dimensions. J Comput Phys 2006;216(1):300–325.
8. Cheng H, Huang J, Leiterman TJ. An adaptive fast solver for the modified Helmholtz equation in two dimensions. J Comput Phys 2006;211(2):616–637.
9. Dutt A, Greengard L, Rokhlin V. Spectral deferred correction methods for ordinary differential equations. BIT 2000;40(2):241–266.
10. Ethridge F, Greengard L. A new fast-multipole accelerated Poission solver in two dimensions. BIT 200;40(2):241–266.
11. Gottlieb, D.; Orszag, SS. Numerical Analysis of Spectral Methods. SIAM; Philadelphia: 1977.
12. Greengard L. Spectral Integration and Two-Point Boundary Value Problems. SIAM J Num Anal 1991;28:1071–1080.
13. Greengard L, Rokhlin V. A Fast Algorithm for Particle Simulations. J Comput Phys 1987;73:325–348.
14. Greengard L, Rokhlin V. A new version of the fast multipole method for the Laplace equation in three dimensions. Acta Number 1997;6:229–269.
15. Hairer, E.; Lubich, C.; Roche, M. The Numerical Solution of Differential-Algebraic Systems by Runge-Kutta Methods. Springer-Verlag; 1989.
16. Hairer, E.; Wanner, G. Solving Ordinary Differential Equations II. Springer; 1996.
17. Huang J, Jia J, Minion ML. Accelerating the Convergence of Spectral Deferred Correction Methods. J of Comp Physics 2006;214(2):633–656.
18. Huang J, Jia J, Minion ML. Arbitrary Order Krylov Deferred Correction Methods for Differential Algebraic Equations. Comput Phys 2007;221(2):739–760.
19. Jia J, Hunag J. Krylov deferred correction accelerated method of lines transpose for parabolic problems. J Comput Phys 2008;227(3):1739–1753.
20. Knoll DA, Keyes DE. Jacobian-free Newton Krylov methods: A survey of approaches and applications. J Comput Phys 2004;193:357–397.

21. Pedit JA, Miller CT. Heterogeneous soprtion processes in subsurface systems. 2 Diffusion modeling approaches. Environmental Science and Technology 1995;29(7):1766–1772.

22. Mergen MRD, Jefferson B, Parsons SA, Jarvis P. Magnetic ion-exchange resin treatment: Impact of water type and resin use. Water Research 2008;42:1977–1988. [PubMed: 18155745]

23. Rangan, A. Deferred Correction Methods for Low Index Differential Algebraic Equations. Preprint

24. Singer PC, Boyer TH, Holmquist A, Morran J, Bourke M. Integrated analysis of NOM removal by magnetic ion exchange. Journal American Water Works Association 2009;101(1):65–73.

25. Wu SC, Gscjwend PM. Numerical modeling of sorption kinectics of organic compounds to soil and sediment particles. Water Resources Reserach 1988;24(8):1373–1383.

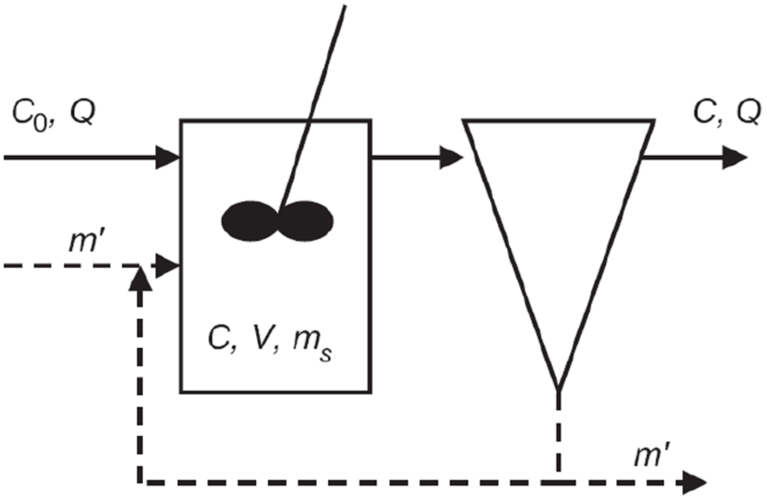

Figure 1.
Continuous flow process schematic

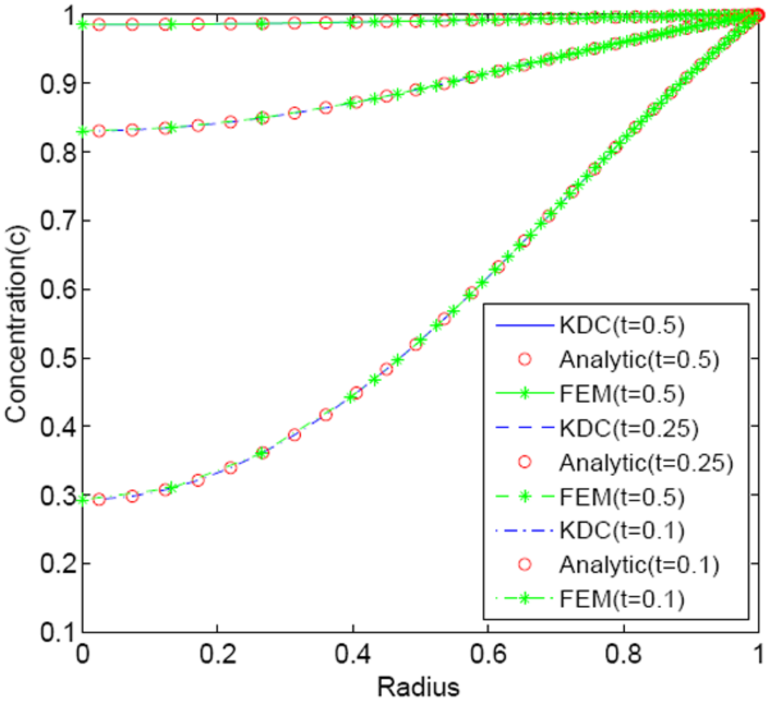

Figure 2.

Comparison of the FEM, KDC, and analytic solutions for diffusion into sphere with a fixed boundary condition.

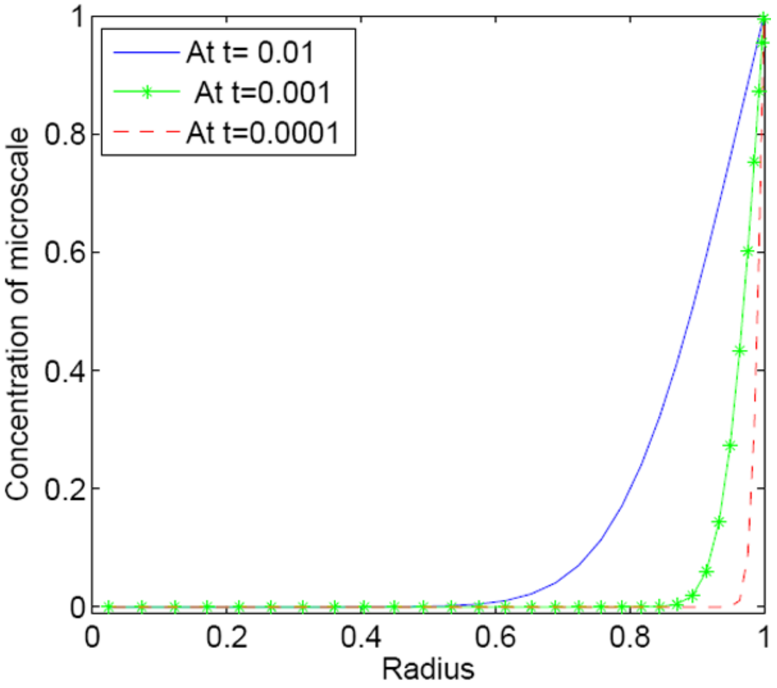

Figure 3.
Comparison of solutions for different initial times.

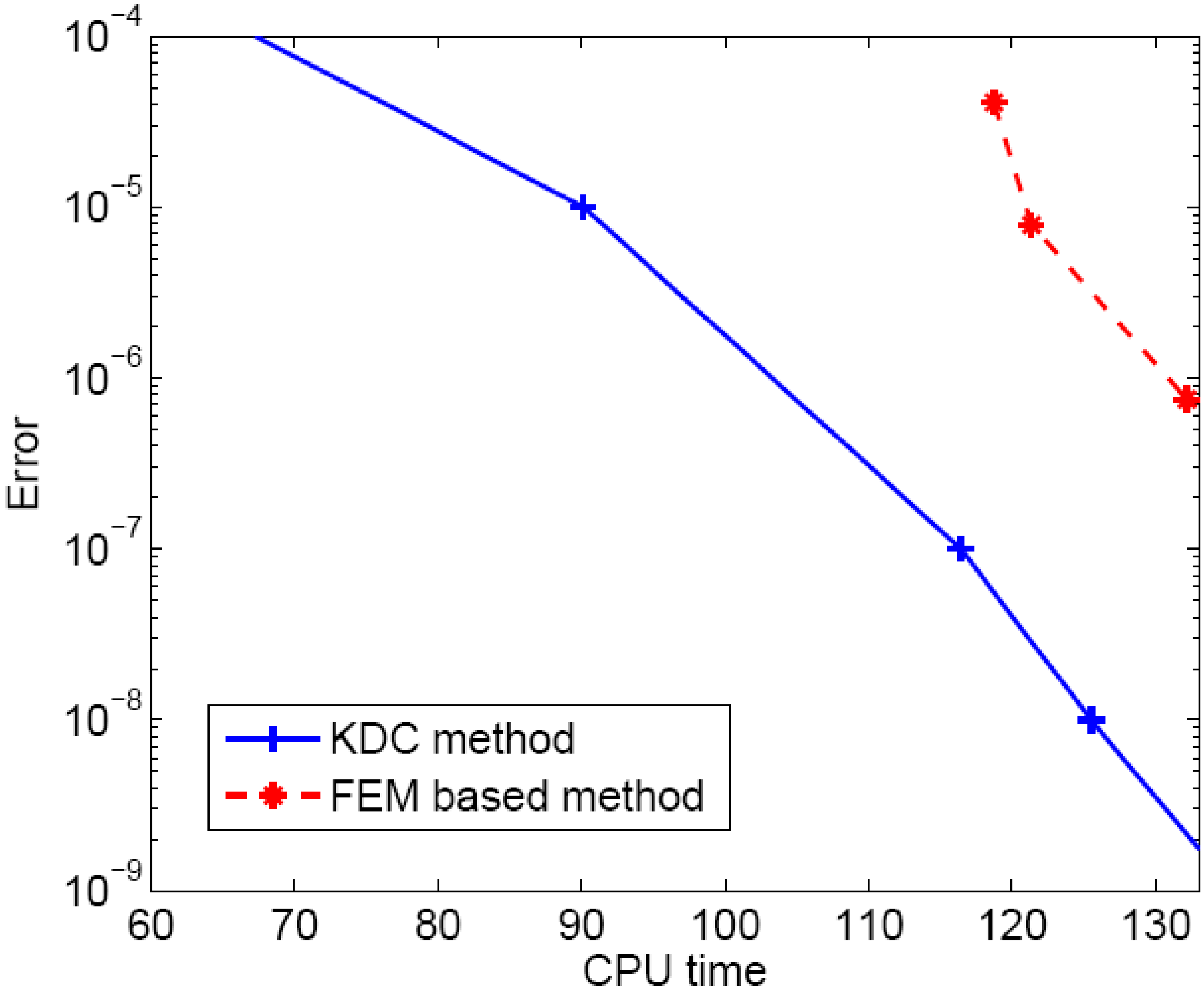

Figure 4.
Comparison of solution efficiency for fixed boundary condition case.

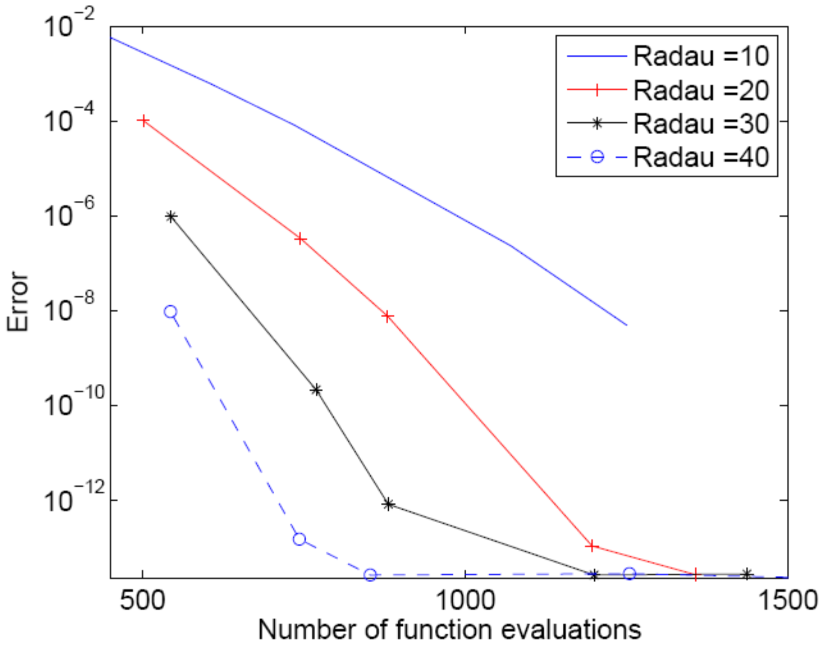

Figure 5.

Accuracy of KDC methods vs. number of function evaluations for varying numbers of Radau nodes.

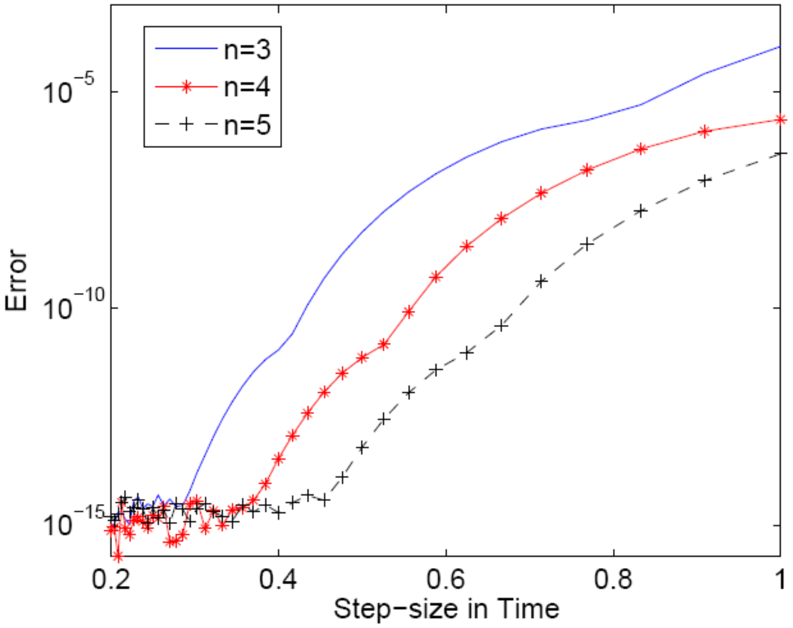

Figure 6.

Accuracy of KDC methods vs. step-size for varying numbers of Radau IIa nodes.

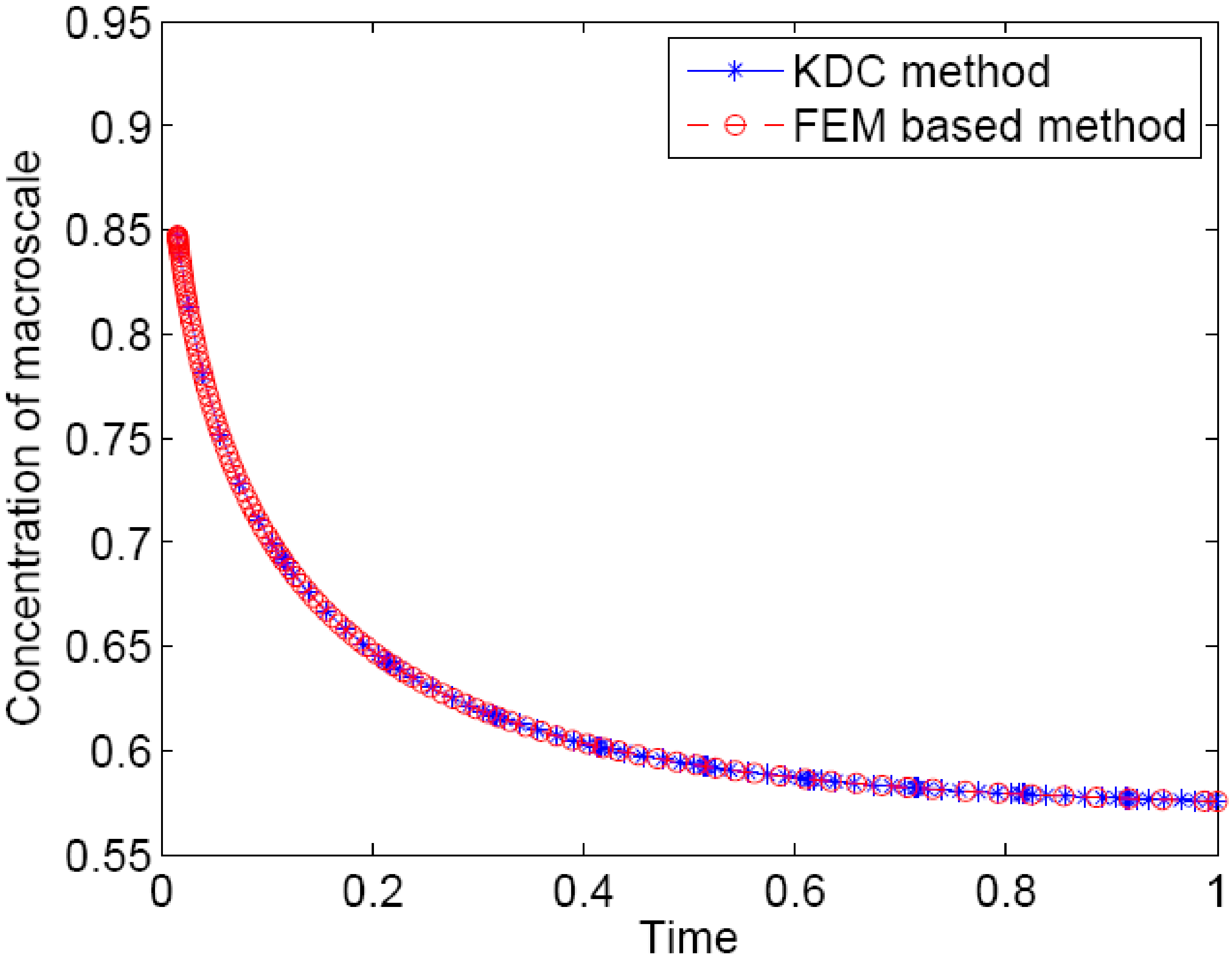

Figure 7.
Comparison of the SI-KDC and FEM solution methods for dynamic boundary conditions.

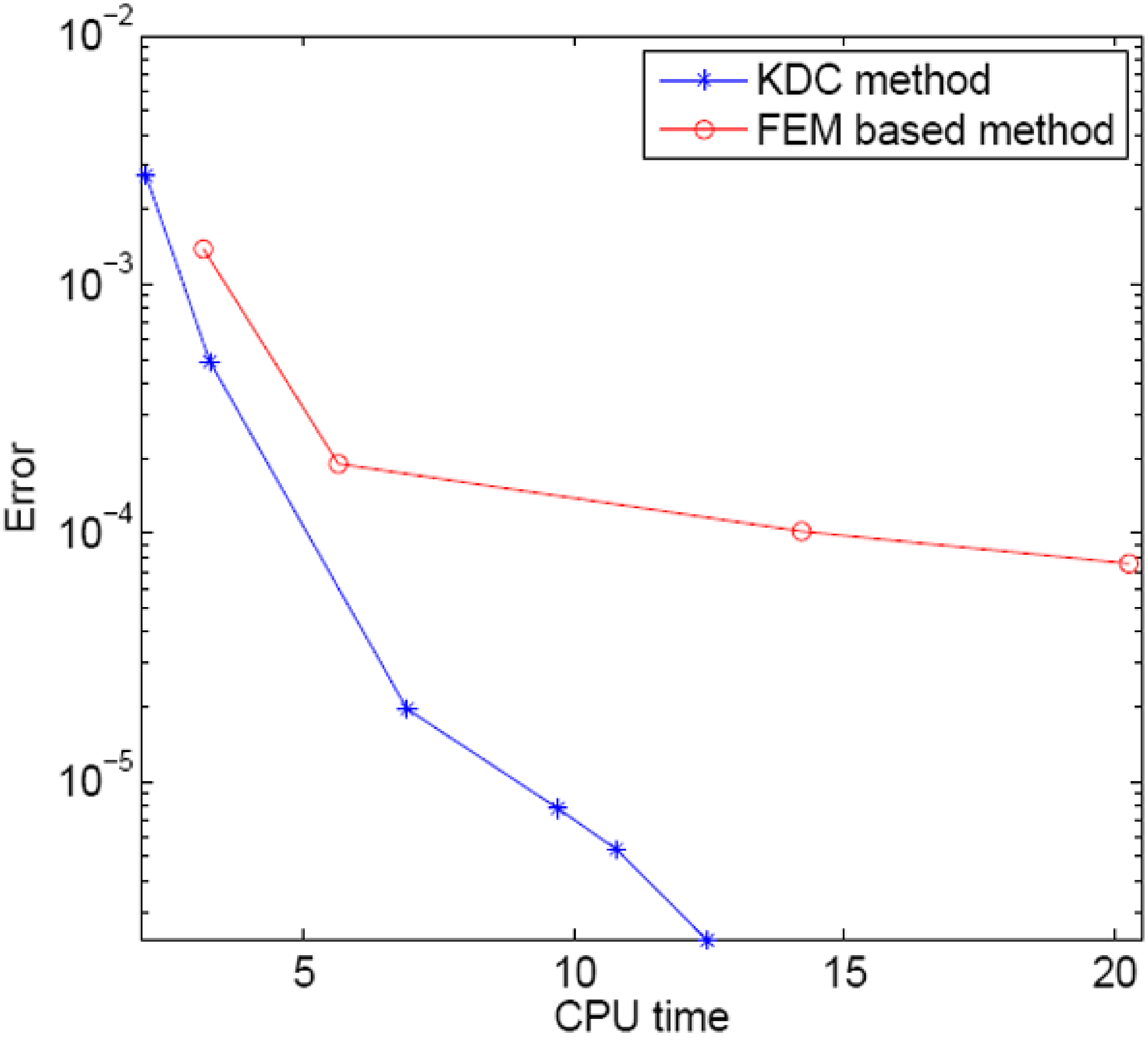

Figure 8.

CPU time comparison for the SI-KDC and FEM solution methods with dynamic boundary conditions.

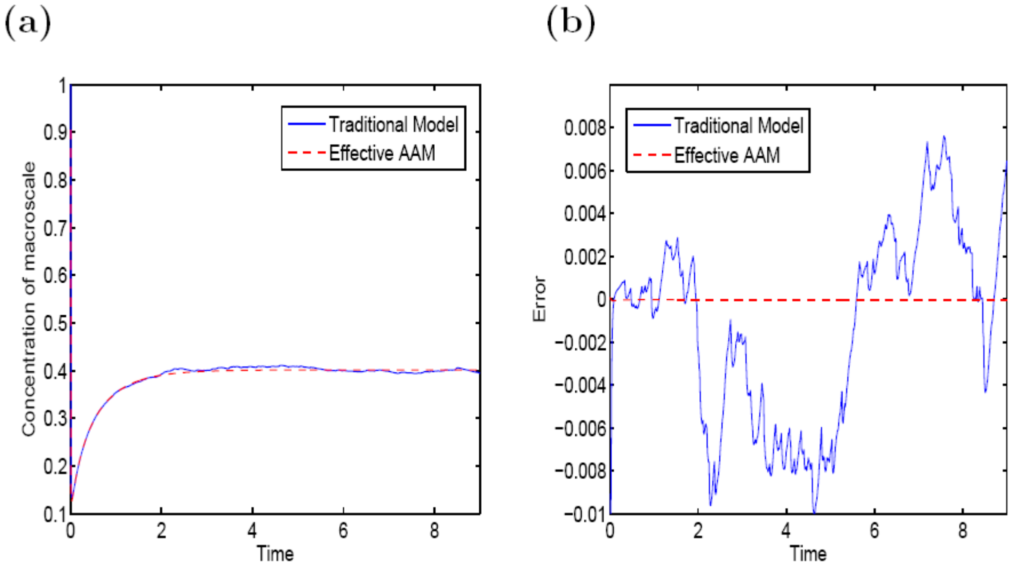

Figure 9.

Comparing traditional two-scale and AAM results(a) and errors (b) using FEM.

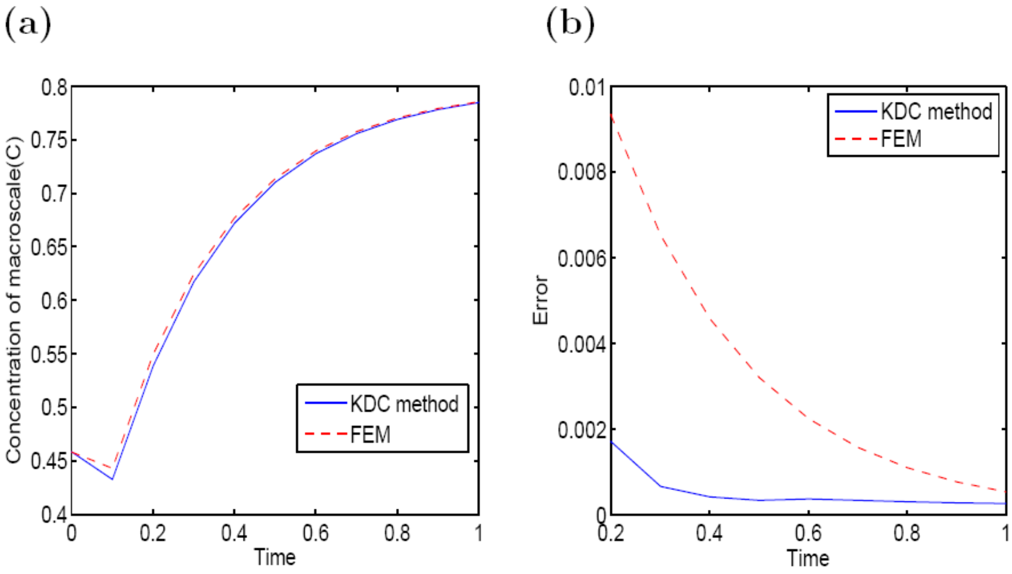

Figure 10.

Comparison of SI-KDC method with FEM based method for the average-aged model with dynamic boundary condition (left) and solution error(right).